SA21B-2519: Modeling the Gradient Drift Instability with Temperature Gradient Effects as Applied to the August 21, 2017 Solar Eclipse Using Two-Fluid Plasma Equations

Chirag Rathod, Bhuvana Srinivasan, Wayne Scales, Gregory Earle

Virginia Tech, Blacksburg, VA, USA

VIRGINIA TECH

Abstract

This work aims to study ionospheric instabilities that may develop significant growth under the conditions of the August 21, 2017 solar eclipse. Evaluating the time-scales of several plasma instabilities, it is hypothesized that the gradient-drift (GDI) instability is likely to develop significant growth during the timespan of a solar eclipse given the relevant gradients that may arise. The two-fluid plasma equations are solved using a finite volume method in the code Gkeyll to understand the growth of the GDI with and without a temperature gradient. The August 21, 2017 solar eclipse conditions are initialized using the International Reference Ionosphere (IRI) and MSIS models. Numerical growth rates are derived for this set of equations for each of these instabilities and are compared to two-fluid plasma simulations as well as to previously published theoretical growth rates. Two-fluid plasma simulations of the GDI show the growth of a secondary instability from the initial perturbation as noted in the ion density but not in the electron density.

Gradient-Drift Instability (GDI)

The gradient-drift instability (GDI) has the possibility of occurring in the presence of a magnetic field, electric field, and a density gradient [5]. The electric field, in these simulations, is assumed to be co-rotational and is replaced by a neutral wind. The difference in collisions with neutral particles between electrons and ions creates a local charge separation that induces electric field perturbations. These smaller electric fields along with the ambient magnetic field cause opposing $E \times B$ drifts along the perturbation with no damping mechanism. Figure 1 shows the orientation for maximum growth of the GDI. There is also a temperature gradient in the same direction as the density gradient that can have an effect on this instability in the solar eclipse.

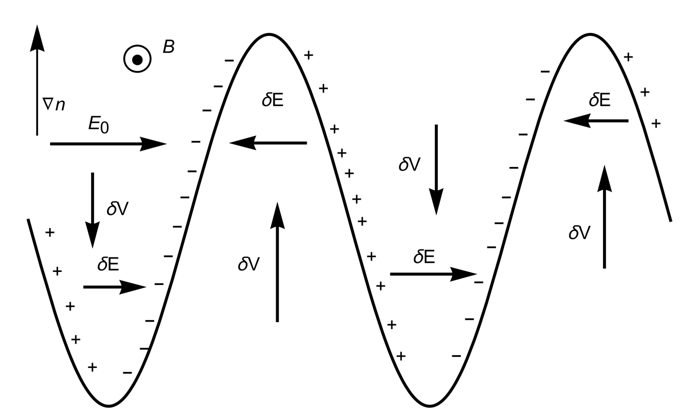

Figure 1: Geometry for maximum GDI growth. The simulation geometry is the same except that a single mode perturbation is initialized.

Orientation of GDI with respect to eclipse

Although the focus is on mid-latitudes, the magnetic field is assumed to be primarily in the up/down direction with a generally northward co-rotating electric field. According to the geometry in Figure 1, the density gradient needs to be generally eastward which would occur on the trailing edge of the umbra.

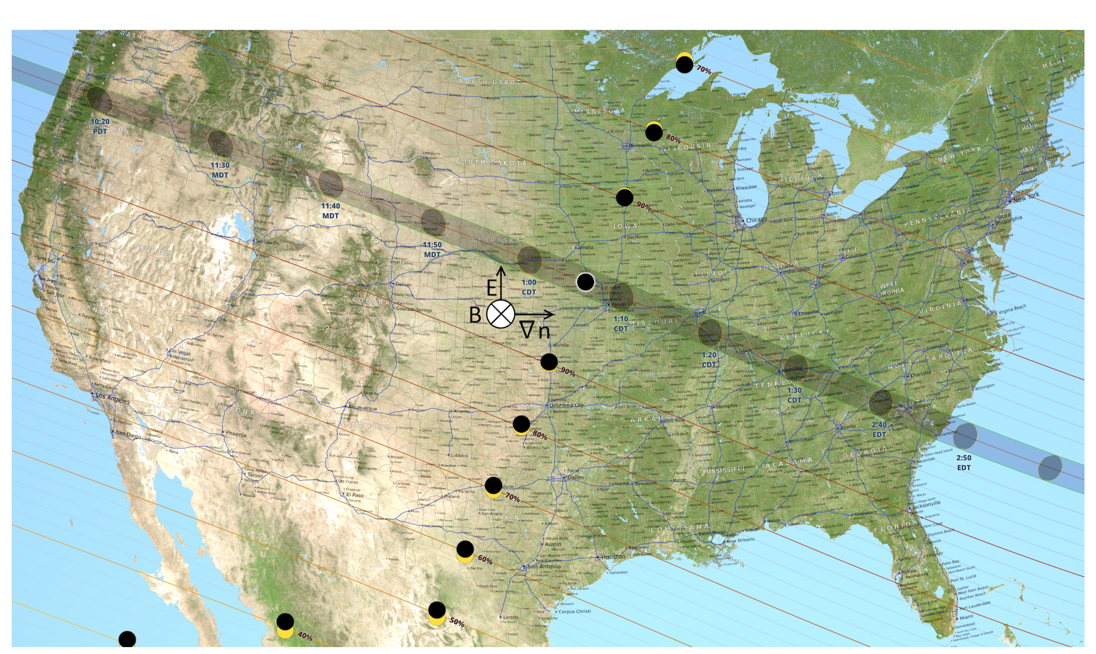

Figure 2: August 21, 2017 solar eclipse map across USA with superimposed conditions for the GDI modified from a visualization by Ernie Wright in conjunction with NASA. URL: https://svs.gsfc.nasa.gov/4518

Two-fluid plasma equations

The two-fluid plasma equations are a combination of two sets of Euler equations, one for electrons and one for ions, and Maxwell's equations with corrections for divergence errors [6]. Ion-neutral and electron-neutral collisions with collision frequency ν_{sn} are included as source terms in the momentum and energy equations. For the following equations, s denotes the species (ion or electron). These equations include energy and electron inertia effects which have been neglected in previous works.

$$\frac{\partial \rho_s}{\partial t} + \nabla \cdot (\rho_s \mathbf{u}_s) = 0 \tag{1}$$

$$\frac{\partial(\rho_s \mathbf{u}_s)}{\partial t} + \nabla \cdot (\rho_s \mathbf{u}_s \mathbf{u}_s) + \nabla p_s = \frac{\rho_s q_s}{m_s}(\mathbf{E} + \mathbf{u}_s \times \mathbf{B}) - \nu_{sn}\rho_s(\mathbf{u}_s - \mathbf{u}_n) \tag{2}$$

$$\frac{\partial \epsilon_s}{\partial t} + \nabla \cdot ((\epsilon_s + p_s)\mathbf{u}_s) = \frac{\rho_s q_s}{m_s}\mathbf{u}_s \cdot \mathbf{E} - \sum_s \frac{1}{2}\nu_{sn}\rho_s(\mathbf{u}_s - \mathbf{u}_n) \cdot (\mathbf{u}_s - \mathbf{u}_n) \tag{3}$$

Where p_s is the pressure found from the ideal gas law and ϵ_s is:

$$\epsilon_s \equiv \frac{p_s}{\gamma - 1} + \frac{1}{2}\rho_s \mathbf{u}_s \cdot \mathbf{u}_s \tag{4}$$

These equations are solved using the finite volume code Gkeyll [1, 2].

Initial conditions, further assumptions, and growth rates

The simulations uses values obtained from the IRI, MSIS, and IGRF models over Sisters, OR at an altitude of 300 km. A weighted average is performed to get an effective ion mass and ion-neutral and electron-neutral collision frequencies. The electric field is assumed to be co-rotational with the magnetic field. The neutral velocity is chosen such that $\mathbf{u}_n \times \mathbf{B} = \mathbf{E}_0$, which in this case points in the positive y direction. The number density is initialized using a hyperbolic tangent with a gradient scale length, L, of 50 m and a change in density of 50%. The plasma is initially quasi-neutral with a single mode perturbation of 2% in both species' densities. Two cases are run: one with the temperature constant throughout the domain and another with the temperature using the same hyperbolic tangent function applied to the density. In both situations, the electron and ion temperatures are not equal. The electron temperature is one order of magnitude larger than the ion temperature.

The following equation is the analytical growth rate for the GDI for a simplified set of equations [4]. More complex analytical formulae exist for the GDI growth but with this geometry and these parameters, it is approximately the Ossakow limit [3].

$$\gamma = \frac{E_0}{BL} \tag{5}$$

Results and Discussion

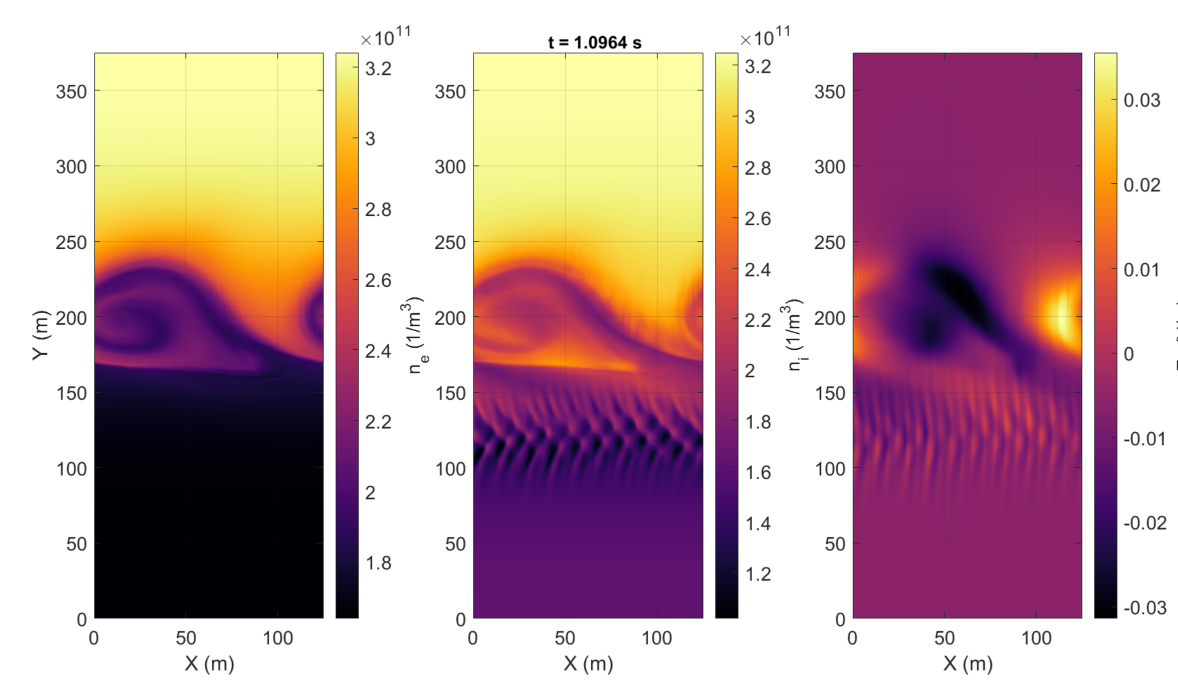

Figure 3: GDI simulation with constant temperature with the electron number density on the left, ion number density in the middle, and x direction electric field on the right at $t = 1.094$ s. The pockets of the predicted oppositely oriented electric fields are seen. Turbulence devlops in the upper part of the domain similar to the development of a Kelvin-Helmholtz instability. A secondary instability forms in the lower part of the domain appearing only in the ion number density and electric field but not in the electron number density.

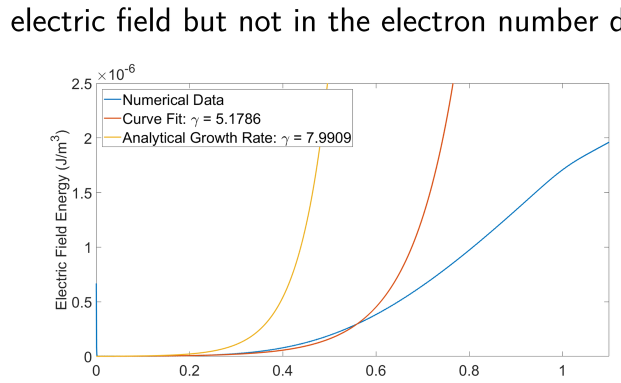

Figure 4: Growth of GDI with constant temperature showing electric field energy as a function of time compared to analytical values. A curve fit for the exponential is applied to the numerical data and compared to the simplified analytical growth rate. Although this is not a perfect comparison because more less assumptions are made in this simulation, it provides a good baseline.

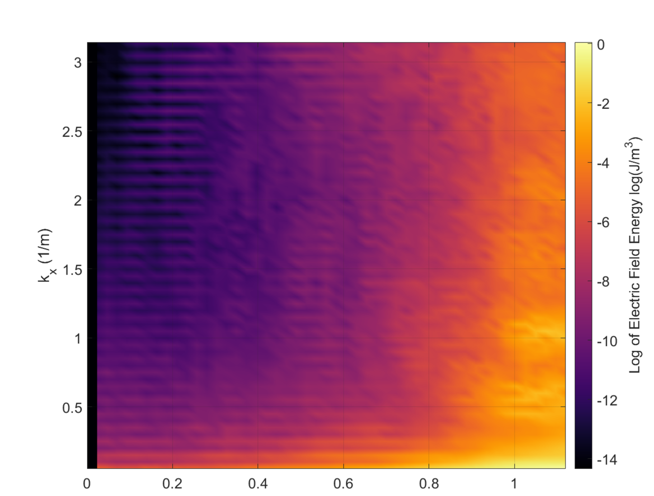

Figure 5: FFT plot showing the log of electric field energy as a function of wave number and time. Initially, only the single mode perturbation is applied. There is a sharp increase in higher modes at around 0.8 s.

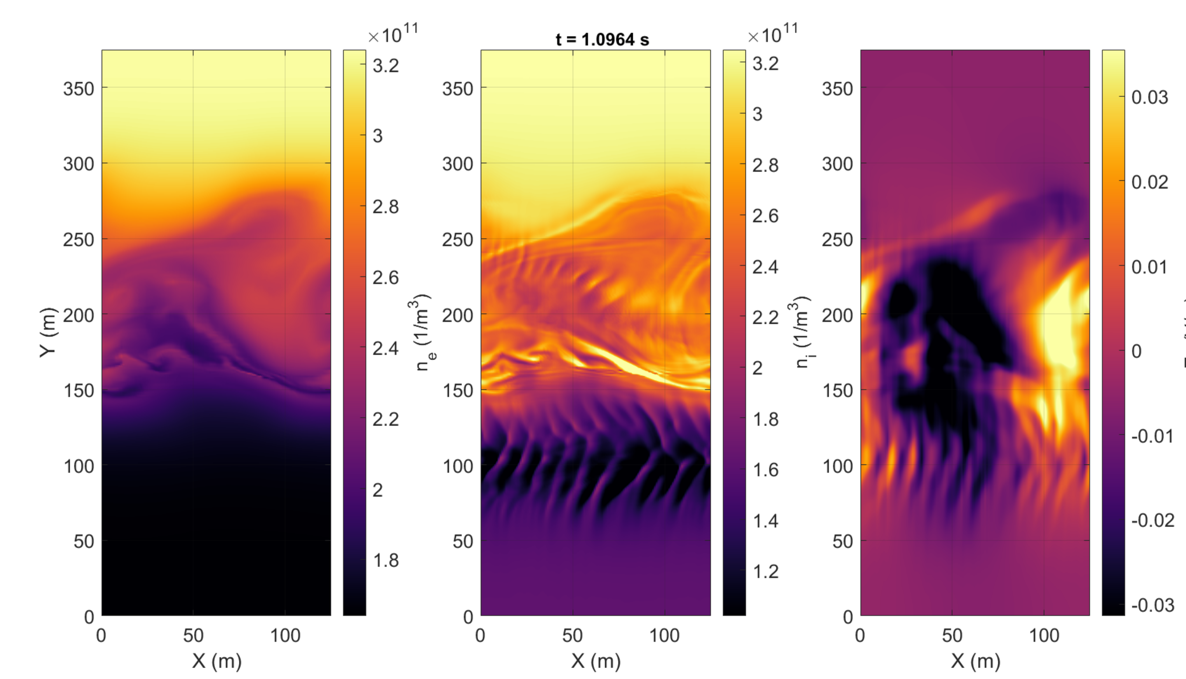

Figure 6: GDI simulation with a temperature gradient with the electron number density on the left, ion number density in the middle, and x direction electric field on the right at $t = 1.094$ s. Similar fluid structures to those found in Figure 3 are found in this simulation with turbulence in the upper domain and a secondary instability in the lower domain. The secondary instabilities also seem to appear on top of the turbulence in the upper region. These secondary instabilities still do not appear in the electron number density.

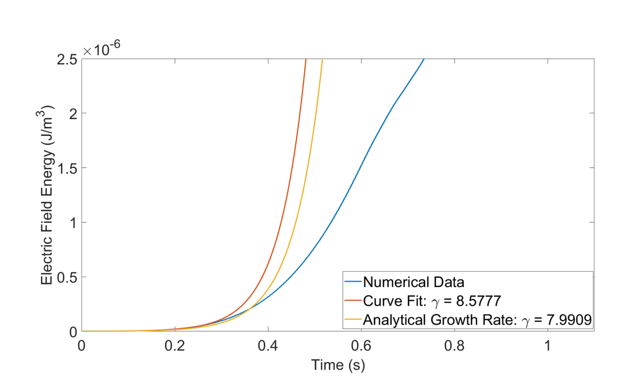

Figure 7: Growth of GDI with constant temperature showing electric field energy as a function of time compared to analytical values. A curve fit for the exponential is applied to the numerical data and compared to the simplified analytical growth rate. The addition of the temperature gradient causes the numerical growth rate to be closer to the analytical growth rate.

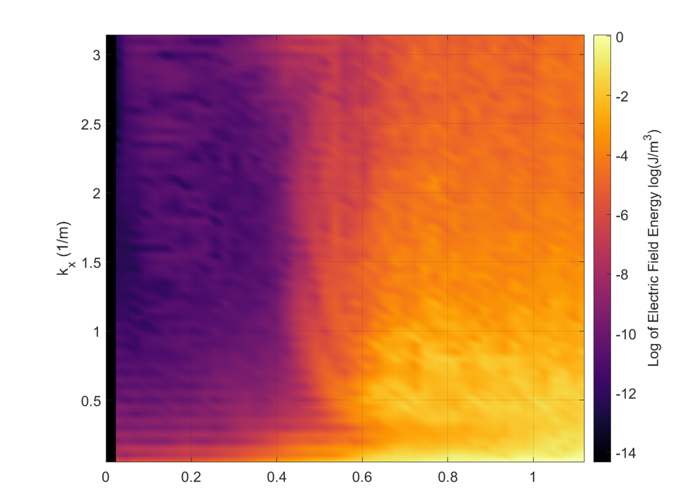

Figure 8: FFT plot showing the log of electric field energy as a function of wave number and time. Initially, only the single mode perturbation is applied. There is a sharp increase in higher modes at around 0.4 s. There is also a different shape to the interface between the lower and higher modes in time in this plot. The temperature gradient causes higher modes to grow much earlier in time.

Table of Initial Conditions

Variable	Value
m_i	2.67×10^{-26} kg
B_{0z}	4.48×10^{-5} T
T_{e0}	2000 K
T_{i0}	880 K
n_0	3.25×10^{11} 1/m^3
ν_{en}	1.07 Hz
ν_{in}	0.542 Hz
u_{ny}	395 m/s

Future Work

Future work will look further into the secondary instabilities present in the GDI. The simulations will be scaled up to look at more realistic solar eclipse length scales and gradient differences. Issues arise due to varying spatial scales from larger eclipse scales compared to the smaller instabilities shown here. The analytical growth rates for both cases will be derived for the full two-fluid plasma equations and compared to previous work. The importance of electron-ion collisions will also be studied.

Summary

The focus of this study is on basic instability physics and how they apply to the August 21, 2017 solar eclipse. The gradient-drift instability has the potential to occur during a solar eclipse in the trailing edge of the umbra. The IRI, MSIS, and IGRF models are used to seed the initial conditions. Cases with both constant temperature and a temperature gradient are simulated to understand their effects on the instability growth. The temperature gradient case is closer to the expected ionospheric conditions during a solar eclipse. Other instabilities and turbulent fluid structures are discovered which are motivations for future work. The growth is comparable to previous work. The case with the temperature gradient displays faster growth and has higher modes develop earlier which shows that a temperature gradient in the same direction as the density gradient is benefical to GDI growth.

Acknowledgements

The authors acknowledge Advanced Research Computing at Virginia Tech for providing computational resources and technical support that have contributed to the results reported within this paper. URL: http://www.arc.vt.edu

Reference

[1] Petr Cagas, Ammar Hakim, James Juno, and Bhuvana Srinivasan. Continuum kinetic and multi-fluid simulations of classical sheaths. *Physics of Plasmas*, 24(2):022118, 2017.

[2] J. Juno, A. Hakim, J. TenBarge, E. Shi, and W. Dorland. Discontinuous galerkin algorithms for fully kinetic plasmas. *Journal of Computational Physics*, 353(Supplement C):110 – 147, 2018.

[3] Roman A Makarevich. Symmetry considerations in the two-fluid theory of the gradient drift instability in the lower ionosphere. *Journal of Geophysical Research: Space Physics*, 119(9):7902–7913, 2014.

[4] SL Ossakow, PK Chaturvedi, and JB Workman. High-altitude limit of the gradient drift instability. *Journal of Geophysical Research: Space Physics*, 83(A6):2691–2693, 1978.

[5] Albert Simon. Instability of a partially ionized plasma in crossed electric and magnetic fields. *The physics of fluids*, 6(3):382–388, 1963.

[6] Bhuvana Srinivasan. *Numerical methods for 3-dimensional magnetic confinement configurations using two-fluid plasma equations*. University of Washington, 2010.